AIP | Applied Physics Letters

# Core-shell Mie resonant structures for quantum computing applications

Roman Shugayev and Peter Bermel

Citation: Applied Physics Letters **109**, 221102 (2016); doi: 10.1063/1.4968806
View online: http://dx.doi.org/10.1063/1.4968806
View Table of Contents: http://scitation.aip.org/content/aip/journal/apl/109/22?ver=pdfcov
Published by the AIP Publishing



# Core-shell Mie resonant structures for quantum computing applications

Roman Shugayev and Peter Bermel[a)]
*Purdue Quantum Center and Birck Nanotechnology Center, 1205 West State Street, Purdue University, West Lafayette, Indiana 47907, USA*

(Received 8 August 2016; accepted 12 November 2016; published online 29 November 2016)

Quantum communications have garnered an increasing amount of interest over the last several years. One of the key components, a deterministic single photon source, requires both high quantum efficiency and suitable emission wavelengths, particularly for ubiquitous fiber-based systems. Solid state single photon sources, comprised of a crystal with isolated, optically active defects, are particularly advantageous in terms of their potential for fine control, reproducibility, ease of operation, and scalability. However, random orientation of single defects presents challenges in terms of scalable manufacturing of such sources. In this paper, we numerically demonstrate Mie resonant core–shell structures that are to a large degree insensitive to random impurity dipole orientations and at the same time decouple spurious decay channels by enhancing both absorption and emission rates. Applying the simple core-shell design to Xenon-related color centers in diamond nanocrystals enhances emission rates into the main zero phonon line by a factor of 23 relative to the bulk diamond. Addition of a Bragg-mirror shell to the Mie core-shell permits a great deal of further increase in the enhancement factor: e.g., a factor of 1273 for a two-bilayer Bragg mirror. A great deal of insensitivity to both the emitting dipole orientation and positioning within the nanocrystal was demonstrated. *Published by AIP Publishing.* [http://dx.doi.org/10.1063/1.4968806]

Quantum photonics is a tremendously promising field likely to revolutionize secure communications and information processing.[1–8] Deterministic single photon sources are an integral part of these emerging technologies and have received significant research attention in the past years.[1,2] There are a number of approaches for producing single photon sources. Systems based on nonlinear spontaneous down-conversion and two level atom systems have been investigated as promising candidates.[3,4] One challenge in these systems is that heralded single photon emission spontaneous down-conversion systems are nondeterministic, which may limit their applicability. Another system recently studied is based on quantum dots, which offer tunability and high emission rates, but can experience fluorescence intermittency, and generally require cryogenic temperature operation.[5]

Atomic or impurity-based systems offer significant advantages for room temperature on-demand single photon sources. In particular, diamond impurity-based solid-state systems have been heavily investigated in the past few years as a potential platform for quantum photonics, including deterministic single photon sources.[6–8] Most recently, optical transitions associated with impurities such as nitrogen vacancies (NV), $H_3$, Si, Xe, and Ni have been studied.

To produce an efficient impurity-based single photon source, it is important to design the proper local environment to selectively enhance zero phonon line (ZPL) emission and/or suppress unwanted decay channels. There are a number of geometries that can enhance the rate of single dipole emission, based on resonant cavity, plasmonic, and near-field effects. However, in these systems, random dipole orientations and positions of the single defect states present a significant challenge for scalable fabrication, as the enhancement is sensitive to the relative orientation of the dipole to the interfaces, which in some cases can completely nullify its benefits. In this paper, we propose and numerically demonstrate a nanocrystal-based device that has the unique property of being largely *insensitive* to the random orientation of the optical center, and at the same time, offering a substantial enhancement of ZPL emission rates over spurious decay channels.

Our basic proposed device consists of a nanocrystal core-shell structure based on magnetic dipole (MD) Mie resonant high-dielectric spheres, tuned to its Mie resonance. Further enhancements of the emission rate are obtained by encapsulating a resonant Mie sphere in the spherical Bragg-mirror multilayer structure. As an example of a technologically relevant system that would greatly benefit from the proposed design, we analyzed absorption and emission for a device consisting of xenon-doped nanodiamonds inside a silicon Mie sphere and inside a combined Mie sphere/Bragg-mirror structure.

The use of MD ZPL lines has been recently suggested as a way to address selective ZPL addressability and readout.[9,10] In general, a number of impurity centers in solid state systems are known to have MD zero phonon emission line. Relevant impurities in dielectric hosts include transitional metals such as Cr:MgO, as well as lanthanide ions.[10,11] In the diamond host, xenon-related centers have been shown to have the same property.[12]

The xenon-related center is a promising single photon source, particularly for fiber based quantum information/communication systems.[8] Ion implantation of Xenon works with a center creation efficiency of approximately 0.3. The Huang-Rhys factor $S$ for the Xe-related center is given by $\exp(-S) = 0.3$ at room temperature.[13,14]

One of the important potential advantages of using a Xe-related center instead of a Si vacancy center is its comparatively favorable location in the fiber optic loss spectrum,

[a)]Author to whom correspondence should be addressed. Electronic mail: pbermel@purdue.edu

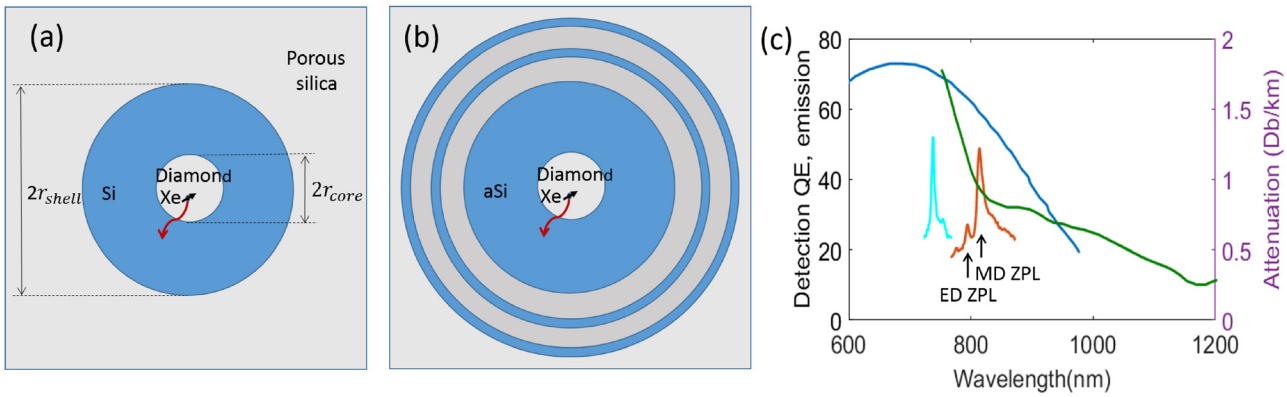


FIG. 1. (a) Core-shell Mie structure. (b) Core-shell structure with added Bragg mirror. (c) Fiber system spectral parameters: the silicon detector quantum efficiency in blue,[8] the fiber attenuation in green,[8] the xenon-related center room temperature emission rate in red,[14] and silicon vacancy room temperature emission rate in cyan.[14]

further into the IR range. This property approximately doubles the maximum distance between directly connected nodes for quantum communication networks [see Figure 1(c)]. This is crucial for secure quantum communication, where losses in the channel become a much stricter constraint. One can potentially offset the increased losses in the classical communication link by retransmission. However, in quantum communications, this is no longer an option, since the eavesdropper can harvest the presumably "lost" photons with their own low-loss communication channel to monitor formerly secure communication channels. This can prove most detrimental for quantum communications using BB84 or similar protocols.

From the point of view of single photon emission, earlier research suggests that Xe-related center emission rates are lower than comparable Si vacancy center rates by approximately two to three orders of magnitude.[14] This is a rough measure of their relative emission rates, and further investigations are needed to better quantify this estimate. Also, at room temperature, the excited state does not radiatively decay exclusively through a single ZPL transition; instead, another ZPL line with $\sigma - \sigma$ electric dipole (ED) transition at $\lambda = 793$ nm emerges.[13] The ratio of emission rates depends on polarization of the main and spurious ZPL lines[13] and is about P(812 nm)/P(793 nm) = 5 for the spectrum shown in Fig. 1(c) in red.

Our concept can greatly enhance far-field emission rates for Xe-related centers, while offering potentially scalable production of such sources. At the same time, since it amplifies only magnetic dipole emission in the system, it would also suppress undesirable electric dipole ZPL decay channels. Additionally, applying this concept to arrays of multiple embedded emitters can lead to quantum array registers[9] with improved optical properties.

In this work, we analyze emitters embedded in resonant Mie spheres, for the purpose of improving their emission rates and selective readout. Dielectric Mie resonators have been studied previously, driven primarily by interest in optical magnetism and scattering,[15–17] as well as dipole emission modification in homogeneous structures.[18,19] The direct approach to enhancing MD single photon emission employing Mie spheres uses a spherical nanocrystal having the radius corresponding to the lowest Mie resonance [Fig. 2(a)]. However, for diamond, it provides a low enhancement relative to bulk emission—roughly a factor of 3. Additionally, the random location and orientation of a single impurity center in such a large crystal do not provide reliable enhancement. The benefits of the suggested core-shell structure [Figure 1(a)] are two-fold. First, this approach greatly amplifies the Mie resonance effect [Fig. 2(a)]. Second, it limits the impurity dipole location to a much smaller radius, sharply reducing the variation of the emission rate observed for the same process.

The silicon shell material was chosen to minimize losses at 812 nm ZPL line, and yet provide high index of refraction needed for enhanced emission. The refractive indices for the

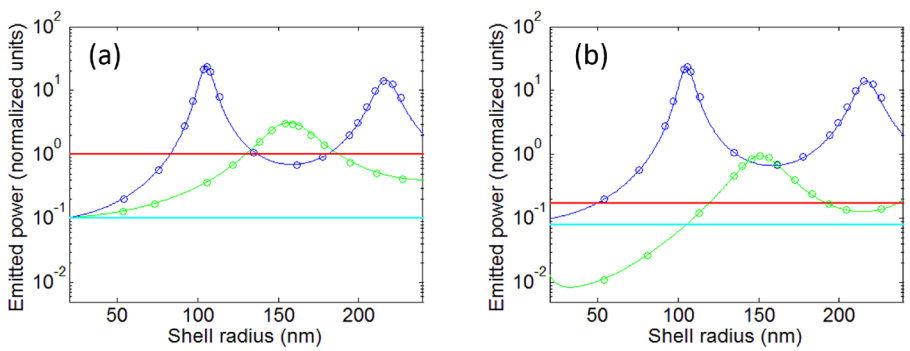


FIG. 2. Normalized emission vs. $r_{shell}$ for $r_{core} = 20$ nm: (a) MD emission of the core-shell structure in blue, of a diamond sphere in green, of homogeneous diamond in red, and of the substrate in cyan; (b) MD emission of the core-shell structure in blue, ED emission of the core-shell structure in green, the homogeneous diamond in red, and the substrate in cyan. Solid lines are analytical results, and circles are FDTD results. Loss free materials are assumed. Emitted power is normalized to bulk diamond magnetic dipole emission.

simulated diamond/silicon structure are $n_1 = 2.4$ and $n_2 = 3.67 + 0.005i$.[20] In all our simulations, we used the finite-difference time domain method using the freely available MEEP package[21] and measured the total emission rate (in arbitrary units, on a consistent scale) by integrating total flux in all directions in the far-field. This approach allows us to calculate that the losses associated with silicon shell absorption for a 20 nm embedded crystal at the ZPL frequency are 2.7%. Alternatively, higher-index materials such as germanium could be used to obtain greater enhancement rates, if the losses were considered acceptable, and the emission rate were the main design constraint. Note that our initial analysis assumes a homogeneous medium of porous silica ($n_3 = 1.1$[22]) to maximize the index contrast with the Mie sphere/multilayer shell structure and to facilitate the comparison with the analytical calculation. Substrate effects are subsequently analyzed.

We also can compare these simulation results with the analytical approach outlined in Ref. 23, and extended as follows. Emission from the core shell structure can be viewed as a two boundary problem in which reflections from the outer boundary can result in modification of the inner boundary conditions. For the case of zero absorption losses and a dipole positioned in the center of the core-shell structure, the governing equations modified for coupling to magnetic modes become

$$\alpha = -i\frac{h_1^{(R)}(z_2)\left(z_1 h_1^{(1)}(z_1)\right)' - h_1^{(1)}(z_1)\left(z_2 h_1^{(R)}(z_2)\right)'}{h_1^{(R)}(z_2)(z_1 j_1(z_1))' - j_1(z_1)\left(z_2 h_1^{(R)}(z_2)\right)'}, \quad (1)$$

$$R = -\frac{h_1^{(1)}(z_3)\left(z_4 h_1^{(1)}(z_4)\right)' - h_1^{(1)}(z_4)\left(z_3 h_1^{(1)}(z_3)\right)'}{h_1^{(2)}(z_3)\left(z_4 h_1^{(1)}(z_1)\right)' - h_1^{(1)}(z_4)\left(z_3 h_1^{(2)}(z_3)\right)'}, \quad (2)$$

where $h_1^{(1)}, h_1^{(2)}$, and $j_1$ are spherical Bessel functions, $h_1^{(R)}(z) = h_1^{(1)} + R h_1^{(2)}(z)$, $K = 1 + \mathrm{Im}(\alpha)$ is the emission rate enhancement factor, $z_i$ are corresponding waves phase shifts defined as $z_1 = k_1 r_{core}$, $z_2 = k_2 r_{core}$, $z_3 = k_2 r_{shell}$, and $z_4 = k_3 r_{shell}$, where $k_i$ are wave numbers in the corresponding media. The imaginary part $\alpha$ represents the additional field acting on the emission center, while $R$ is the coefficient of reflection of the spherical wave from the outer Mie sphere boundary.

The resonance occurs when the real part of denominator of Equation (2) is minimized, which for the lowest order MD resonance corresponds to $r_{shell} \approx \lambda/2n_{shell}$. The shell radii associated with the magnetic and electric dipole Mie resonances are well separated [Figure 2(b)], which results in an MD to ED emission ratio of 286. Using the parameters of experimental results from bulk diamond, the modified ratio is $\mathrm{P}(812\mathrm{nm})/\mathrm{P}(793\mathrm{nm}) = 5 \cdot 286/n_1^2 = 248.3$, as we consider that ED and MD emission ratios scale as $n$ and $n^3$, respectively.[24]

In the case of the core/shell structure with nanocrystals positioned in the center of the Mie sphere, additional boundary conditions having the same symmetry imposed by the nanocrystal/nanoshell interface will not perturb resonant frequencies. For example, when $r_{core} = 40$ nm, the change is 0.6%. Increasing the radius of the nanocrystal reduces emission rates, since less energy is stored inside the shell region [Figure 3(a)]. The decrease in emission is gradual, as the alpha term in Equation (1) is smoothly varying for $r_{core} \ll r_{shell}$. We find that the enhancement factors for the core/shell structure versus the homogeneous diamond and the homogeneous diamond versus the substrate are 23 and 7.6, respectively [Figure 2(a)] for $r_{core} = 20$ nm and $r_{shell} = 105$ nm. Shifting the position of the dipole emitter from the center also reduces the emission rate for both azimuthally polarized emissions and radially polarized emissions. Assuming the worst case of azimuthally polarized emission for a nanocrystal with $r_{core} = 20$, the maximum reduction in the emission rate is only 8%. This number can be further reduced for smaller nanocrystal radii.

Additionally, we can consider the effects of a non-ideal crystal geometry. Looking at the extreme case where the nanocrystal changes from a sphere to a cube, the eigenmodes of two boundaries are significantly mismatched, thus reducing the emission more than expected [Figure 3(a)]. For small nanocrystal dimensions (<20 nm), this effect reduces emission <8%; at a nanocrystal radius of 40 nm, the maximum reduction is <25%. The total emission rate depends very little on the exact orientation of the emitting dipole within the nanocube crystal; the variation of the emission rate in our simulation is <0.1%.

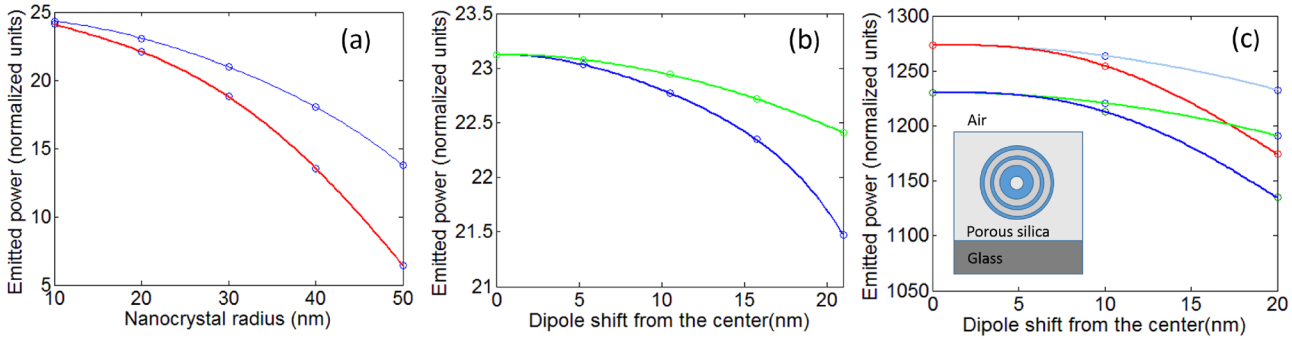


FIG. 3. (a) Emission vs. core radius $r_{core}$: (blue) core-shell nanocrystal structure and (red) core-shell structure with a cubic nanocrystal. (b) Emission vs. distance of the dipole from the center, given $r_{core} = 20$ nm. (c) Emission vs. distance for a Mie sphere/Bragg mirror 2-layer structure. The free-standing structure results (no substrate) are in red and cyan; the results with a glass substrate are in green and blue. (Inset) Simulated Mie sphere/multilayer structure on a top glass substrate. In (b) and (c), blue and red represent azimuthally oriented dipole emission, while green and cyan represent radial dipole emission (all in the Mie sphere coordinate system).

To increase the cavity Purcell factor and corresponding emission rates, we can encapsulate the efficient Mie sphere-design within a Bragg mirror-like spherical multilayer structure [Figure 1(b)]. This modifies the effective reflection coefficient $R$, which permits higher energy confinement. The insensitivity of the emission rate to the position and orientation of the emitting dipole is maintained; for a double bilayer Bragg mirror, we obtain emission enhancement of a factor of 1273 [Figure 3(c)]. To minimize material losses and corresponding Q reduction, amorphous silicon (a-Si) with a refractive index $n_2 = 3.4 + 5 \cdot 10^{-5} i$[25] is used for the high-index Bragg mirror layers as well as the Mie sphere. The losses due to absorption in a-Si were found to be 3.2%. The interlayer spacer was assumed to be porous silica. The layer thicknesses were taken as 43 nm and 233 nm for a-Si and porous silica, respectively, with $r_{core} = 20$ nm and $r_{shell} = 115.6$ nm. Using this method, even larger increase in emission rate could potentially be achieved with a greater number of Bragg mirror periods. However, such an increase comes at the expense of increased fabrication complexity and material losses.

Effects of the substrate were analyzed by substituting semi-infinite air $n_{air} = 1$ and glass $n_{sub} = 1.45$ at a distance of one wavelength above and below the structure, respectively, as shown in the inset in Fig. 3(c). Inclusion of the substrate reduces the overall emission by 3.5%, while still maintaining position/orientation insensitivity. The small influence of the substrate on overall emission is attributed to the relatively small index mismatch between porous silica and a substrate that minimizes back-reflections at the boundary.

To optically pump a single Xe-related center at the ZPL transition, several excitation energies can be used.[12–14] Assuming a 690 nm plane wave excitation (corresponding to electric dipole absorption), we find that the core electric field intensities in the simple Mie sphere structure increase by a factor of 2, relative to the medium, which corresponds to a factor of 0.9 in the bulk diamond. Alternatively, the structure can also be excited using resonant magnetic dipole ZPL transitions. The corresponding absorption rates are increased as much as a factor of 208 times relative to the medium, with the maximum enhancement coinciding with the nanoparticle center.

While here we presented an example of a system with an MD dipole separating the main ZPL from spurious decay channels, this proposed methodology can also be applied to ED vacancy systems, such as NV centers, for direct enhancement of fluorescence rates. Without considering losses, the enhancements would decrease by a factor of 1.65 [Figure 2(b)], and the overall dimension of the system would increase by a factor of 1.5 for the analyzed core-shell Mie structure. However, since most high index materials absorb more at the shorter NV transition wavelengths (637 nm for the ZPL), achievable emission rate enhancements would be reduced. On the other hand, this method can readily be used to enhance the weak IR fluorescence of the NV center at 1042 nm.[26]

Another important goal for quantum computing is to realize entangled quantum registers. Structured nanodiamond arrays coupled via nearest neighbor spin interactions have recently been demonstrated.[27] Still, this coupling is limited by the coherence time of the interaction, which restricts the distance between individual emitters to 20–30 nm. It is desirable to scale this methodology to arrays of emitters for implementation of large, scalable quantum registers. From the perspective of optical readout, it is important to provide high rate fluorescence while monitoring the state change in such networks. It is also desirable to utilize unique microwave addressing frequencies for each element in a coupled array. The bulk diamond can only provide few microwave addressing frequencies for the impurities, since they occupy a set of crystal orientations. Therefore, we can consider embedding discrete nanocrystals having single vacancies arranged in 1D, 2D, or 3D patterns inside the single Mie sphere. Our results show that increasing the number of particles from one to 27 only changes the emission rate for the dipole emitter positioned in the center by 7%, while maintaining high emission enhancement [Figure 4(a)]. Particles with $r_{core} = 10$ nm are assumed to be equally spaced by a 20 nm in geometries forming a line (3 particles), a plane (9 particles), or a cube (27 particles), positioned about the center of the Mie sphere and closely packed.

It is also advantageous to achieve selective fluorescent readout from individual nanocrystals in such embedded arrays. Figure 4(b) shows the transition energy shift computed using $\frac{\omega-\omega_0}{W_1} = \frac{1}{2}\mathrm{Re}(\alpha)$, where $W_1$ is the natural linewidth of the oscillator in the medium with refractive index $n_1$.[22,28] The change of frequency in the vicinity of the resonance is greater for the MD dipole than the ED dipole by a factor of 4.88. Such an energy shift can potentially be used for the selective readout of the state of quantum register arrays, particularly at the low temperatures. In addition, this effect can be used for tuning of emission frequency and determination of exact particle dimensions as an alternative to microscopy methods.

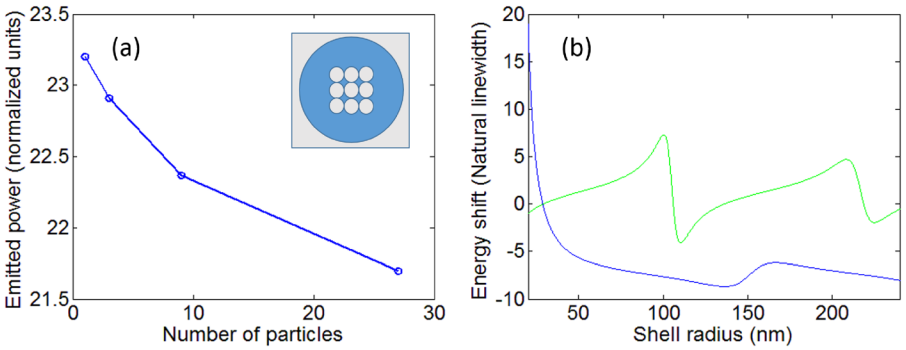


FIG. 4. (a) Emitted power versus number of embedded nanocrystal particles, arranged in a closely packed array (inset), the geometry for the 27 particle array simulated. (b) Energy shift of the transition for the cases of MD (green) and ED (blue) emission. The emitter is assumed to be centered at the origin.

Future research should focus on the fabrication and characterization of the proposed core-shell structures. Core-shell structures with controlled shell thickness and uniformity can be fabricated[29,30] using sol-gel techniques. The porous silica matrix could be produced using techniques for low-k material fabrication.[31] Embedding very small nanoparticles in the mesoporous silica matrices has been reported in the literature.[32] Commercially produced nanodiamonds would be doped with Xe using ion implantation, as discussed above.[12,13,33] Core-shell structures have also been demonstrated using scalable techniques like fiber drawing, but further investigation may be needed to successfully incorporate nanodiamonds.[34]

In conclusion, we have demonstrated that the core-shell Mie resonant structures offer a significant enhancement of emission rates of embedded single defect sources. They show a high degree of emission isotropy and emission selectivity, thus providing a paradigm for managing the experimental variability of the solid-state vacancy orientation and positioning. The proposed core-shell Mie sphere designs can bridge the technological gap between research and production of bright, solid-state single-photon sources. Furthermore, arrays of embedded nanocrystals can potentially be utilized as quantum register systems for communications or information processing, with significantly enhanced emission rates and selective readout capabilities.

The authors thank Sattwik Deb Mishra, Mikhail Shalaginov, and Simeon Bogdanov for valuable discussions. Support was provided by the National Science Foundation, under Award No. EEC1454315-CAREER: Thermophotonics for Efficient Harvesting of Waste Heat as Electricity.

[1]M. D. Eisaman, J. Fan, A. Migdall, and S. V. Polyakov, Rev. Sci. Instrum. **82**, 071101 (2011).
[2]L. Brahim and M. Orrit, Rep. Prog. Phys. **68**, 1129 (2005).
[3]F. Sylvain, O. Alibart, S. Tanzilli, P. Baldi, A. Beveratos, N. Gisin, and H. Zbinden, New J. Phys. **6**, 163 (2004).
[4]T. B. Pittman, B. C. Jacobs, and J. D. Franson, Opt. Commun. **246**, 545 (2005).
[5]S. Buckley, K. Rivoire, and J. Vučković, Rep. Prog. Phys. **75**, 126503 (2012).
[6]T. M. Babinec, B. J. M. Hausmann, M. Khan, Y. Zhang, J. R. Maze, P. R. Hemmer, and M. Lončar, Nat. Nanotechnol. **5**, 195 (2010).
[7]L. J. Rogers, K. D. Jahnke, T. Teraji, L. Marseglia, C. Müller, B. Naydenov, H. Schauffert, C. Kranz, J. Isoya, L. P. McGuiness, and F. Jelezko, Nat. Commun. **5**, 4739 (2014).
[8]S. Pezzagna, D. Rogalla, D. Wildanger, J. Meijer, and A. Zaitsev, New J. Phys. **13**, 035024 (2011).
[9]R. Shugayev and P. Bermel, Appl. Phys. Lett. **108**, 071106 (2016).
[10]S. Karaveli, S. Wang, G. Xiao, and R. Zia, ACS Nano **7**, 7165 (2013).
[11]P. A. Tanner, "Lanthanide luminescence in solids," in *Lanthanide Luminescence* (Springer, Berlin, Heidelberg, 2010), pp. 183–233.
[12]Y. Dziashko, see http://academicworks.cuny.edu/gc_etds/483 for "Optical spectroscopy of xenon-related defects in diamond," All Dissertations, Theses, and Capstone Projects (2014-Present), Paper No. 483, 2014.
[13]Y. Deshko and A. A. Gorokhovsky, Low Temp. Phys. **36**, 465 (2010); A. A. Bergman, A. M. Zaitsev, and A. A. Gorokhovsky, J. Lumin. **125**, 92 (2007).
[14]C. Wang, "A solid-state single photon source based on color centers in diamond," PhD dissertation (LMU Munich, 2007).
[15]Q. Zhao, J. Zhou, F. Zhang, and D. Lippens, Mater. Today **12**, 60 (2009).
[16]A. I. Kuznetsov, A. E. Miroshnichenko, Y. H. Fu, J. Zhang, and B. Luk'Yanchuk, Sci. Rep. **2**, 492 (2012).
[17]Y. H. Fu, A. I. Kuznetsov, A. E. Miroshnichenko, Y. F. Yu, and B. Luk'yanchuk, Nat. Commun. **4**, 1527 (2013).
[18]X. Zambrana-Puyalto and N. Bonod, Phys. Rev. B **91**, 195422 (2015).
[19]H. Chew, "Transition rates of atoms near spherical surfaces," J. Chem. Phys. **87**, 1355 (1987).
[20]M. A. Green and M. J. Keevers, Prog. Photovoltaics **3**, 189 (1995).
[21]A. F. Oskooi, D. Roundy, M. Ibanescu, P. Bermel, J. D. Joannopoulos, and S. G. Johnson, Comput. Phys. Commun. **181**, 687 (2010).
[22]Y. Zhang, C. Zhao, P. Wang, L. Ye, J. Luo, and B. Jiang, Chem. Commun. **50**, 13813 (2014).
[23]V. V. Klimov and V. S. Letokhov, "Enhancement and inhibition of spontaneous emission rates in nanobubbles," Chem. Phys. Lett. **301**, 441 (1999).
[24]G. L. J. A. Rikken and Y. A. R. R. Kessener, Phys. Rev. Lett. **74**, 880 (1995).
[25]G. D. Cody, C. R. Wronski, B. Abeles, R. B. Stephens, and B. Brooks, Sol. Cells **2**, 227 (1980).
[26]V. M. Acosta, A. Jarmola, E. Bauch, and D. Budker, Phys. Rev. B **82**, 201202(R) (2010).
[27]A. Albrecht, G. Koplovitz, A. Retzker, F. Jelezko, S. Yochelis, D. Porath, Y. Nevo, O. Shoseyov, Y. Paltiel, and M. B. Plenio, New J. Phys. **16**, 093002 (2014).
[28]V. V. Klimov, M. Ducloy, and V. S. Letokhov, J. Mod. Opt. **43**, 549 (1996).
[29]K. P. Velikov and A. van Blaaderen, Langmuir **17**, 4779 (2001).
[30]M. Ammar, F. Mazaleyrat, J. Bonnet, P. Audebert, A. Brosseau, G. Wang, and Y. Champion, "Synthesis and characterization of core–shell structure silica-coated $Fe_{29.5}Ni_{70.5}$ nanoparticles," Nanotechnology **18**, 285606 (2007).
[31]S. Kuck, L. Fornasiero, E. Heumann, E. Mix, G. Huber, T. Karner, and A. Maaroos, Laser Phys. **10**, 411 (2000).
[32]L. Wang, J. Shi, Y. Zhu, Q. He, H. Xing, J. Zhou, F. Chen, and Y. Chen, Langmuir **28**, 4920 (2012).
[33]A. P. Koscheev, M. D. Gromov, P. V. Gorokhov, U. Ott, G. R. Huss, and T. L. Daulton, Meteorit. Planet. Sci. **40**, A87 (2005), Abstract 5337.
[34]J. J. Kaufman, T. Guangming, S. Soroush, E.-H. Banaei, D. S. Deng, X.-D. Liang, S. G. Johnson, Y. Fink, and A. F. Abouraddy, "Structured spheres generated by an in-fibre fluid instability," Nature **487**, 463 (2012).